

Large-eddy simulation of flow over a wall-mounted hump with separation control

By D. You, M. Wang AND P. Moin

1. Motivation and objectives

Over the past several decades various active flow control concepts have been proposed and evaluated to improve the efficiency and stability of aero-/hydro-dynamic systems such as turbomachines and road/flight vehicles. Many of these techniques involve continuous blowing or suction, which can produce effective control but is difficult to apply in real fluid systems. In recent years, control devices involving zero-net mass-flux oscillatory jets or synthetic jets have shown feasibility for industrial applications and effectiveness in controlling flow separation (Glezer & Amitay 2002; Rumsey *et al.* 2004; Seifert & Pack 2002; Greenblatt *et al.* 2004, 2005; Šarić *et al.* 2005; Krishnan *et al.* 2004; Capizzano *et al.* 2005; Morgan *et al.* 2004, 2005; Postl *et al.* 2004).

An accurate prediction, not to mention control, of unsteady flow separation at high Reynolds numbers is a challenging task for numerical simulations. Recently, a broad range of numerical techniques such as large-eddy simulation (LES) with a constant Smagorinsky model (Šarić *et al.* 2005), detached eddy simulation (DES) (Krishnan *et al.* 2004), steady or unsteady Reynolds-averaged Navier-Stokes (RANS or URANS) simulations (Capizzano *et al.* 2005; Morgan *et al.* 2004; Krishnan *et al.* 2004), implicit LES (ILES) (Morgan *et al.* 2005), and direct numerical simulation (DNS) (Postl *et al.* 2004) have been utilized to predict the turbulent separation and its control over a wall-mounted hump at $Re = 9.36 \times 10^5$, where the Reynolds number is based on the hump chord C and freestream velocity U_∞ . This flow configuration is one of the test cases considered in the NASA Workshop on Synthetic Jets and Turbulent Separation Control (Rumsey *et al.* 2004; Seifert & Pack 2002; Greenblatt *et al.* 2004, 2005). None of the RANS techniques gave satisfactory prediction of the important flow features such as the size of the separation bubble, the pressure coefficient on the hump surface, and the mean velocity and turbulence intensity profiles (Capizzano *et al.* 2005; Morgan *et al.* 2004; Krishnan *et al.* 2004; Rumsey *et al.* 2004). The DNS results of Postl *et al.* (2004) were unsatisfactory due to the use of unrealistic inflow velocity profiles and insufficient grid resolution and spanwise domain size. Morgan *et al.* (2005) obtained better agreement with experimental data using ILES. However, the Reynolds number employed in the ILES is only about one-fifth of the experimental Reynolds number. While the DES predictions of Krishnan *et al.* (2004) were much better compared to their RANS results, discrepancies with experimental data (Seifert & Pack 2002) were still significant. Šarić *et al.* (2005) reported that the LES with a constant Smagorinsky model can provide good predictions in the uncontrolled baseline and steady suction control cases, while it exhibits significant deviations of mean velocity profiles from the experimental data (Greenblatt *et al.* 2004, 2005) in the oscillatory jet (modeled synthetic jet) case.

In this study, we employ LES with a dynamic subgrid-scale model (Germano *et al.* 1991) and non-dissipative numerics to predict the turbulent flow separation and its control by synthetic jets in the same hump-model configuration. The dynamic subgrid-scale

model, which has been shown to produce good results in a number of complex turbulent flow simulations (You *et al.* 2004a; Wang & Moin 2000; Kaltenbach *et al.* 1999; Wu & Squires 1998; Mittal & Moin 1997), is employed. In contrast to the LES techniques that employ upwind-biased schemes (Sarić *et al.* 2005) or the ILES (Morgan *et al.* 2005), which relies on numerical dissipation or high-order spatial filtering to play the role of a subgrid-scale model, the present LES utilizes an energy-conservative second-order central difference scheme on a staggered mesh (You *et al.* 2004a; Choi *et al.* 1992). Aliasing errors are controlled by enforcing kinetic energy conservation, not by numerical dissipation or filtering, and artificial damping of small scales is avoided. This feature is particularly important for successful LES of turbulent flows (Mittal & Moin 1997; Beaudan & Moin 1994).

The present LES has produced superior results compared to those obtained from previous simulations (Capizzano *et al.* 2005; Morgan *et al.* 2004; Krishnan *et al.* 2004; Postl *et al.* 2004; Morgan *et al.* 2005; Rumsey *et al.* 2004) for both controlled and uncontrolled cases. Detailed comparisons of mean and turbulence statistics such as the pressure coefficient, skin friction coefficients, and velocity and Reynolds stress profiles are presented. The effects of steady suction and oscillatory jet on flow separation and reattachment are discussed.

2. Computational methodology

2.1. Numerical method

The numerical algorithm and solution methods are described in detail in Refs. Choi *et al.* (1992) and You *et al.* (2004b), and the main features of the methodology are summarized here. The spatially filtered Navier-Stokes equations for resolved scales in LES are as follows:

$$\frac{\partial \bar{u}_i}{\partial t} + \frac{\partial}{\partial x_j} \bar{u}_i \bar{u}_j = -\frac{\partial \bar{p}}{\partial x_i} + \frac{1}{\text{Re}} \frac{\partial}{\partial x_j} \frac{\partial \bar{u}_i}{\partial x_j} - \frac{\partial \tau_{ij}}{\partial x_j}, \quad (2.1)$$

$$\frac{\partial \bar{u}_i}{\partial x_i} = 0, \quad (2.2)$$

where τ_{ij} is the subgrid scale (SGS) stress tensor. All the coordinate variables, velocity components, and pressure are nondimensionalized by the hump cord length C , the inflow freestream velocity U_∞ , and ρU_∞^2 , respectively. The time is normalized by C/U_∞ . The governing equations (2.1) and (2.2) are rewritten in a conservative form in generalized coordinates. The dependent variables in the transformed Navier-Stokes equations are volume fluxes across the faces of computational cells, which are equivalent to the use of the contravariant velocity components on a staggered grid multiplied by the Jacobian of the coordinate transformation. With this choice of variables, the discretized mass conservation can easily be satisfied. The terms in the transformed equations are described in detail in Ref. You *et al.* (2004b). The key feature of the numerical method is the use of a non-dissipative, central-difference spatial discretization scheme which has been demonstrated to be crucial for retaining the accuracy and predictive capability of the LES (Mittal & Moin 1997).

The SGS stress tensor τ_{ij} is modeled by a Smagorinsky type eddy-viscosity model:

$$\tau_{ij} - \frac{1}{3} \delta_{ij} \tau_{ij} = -2c \Delta^2 |\bar{S}| \bar{S}_{ij}. \quad (2.3)$$

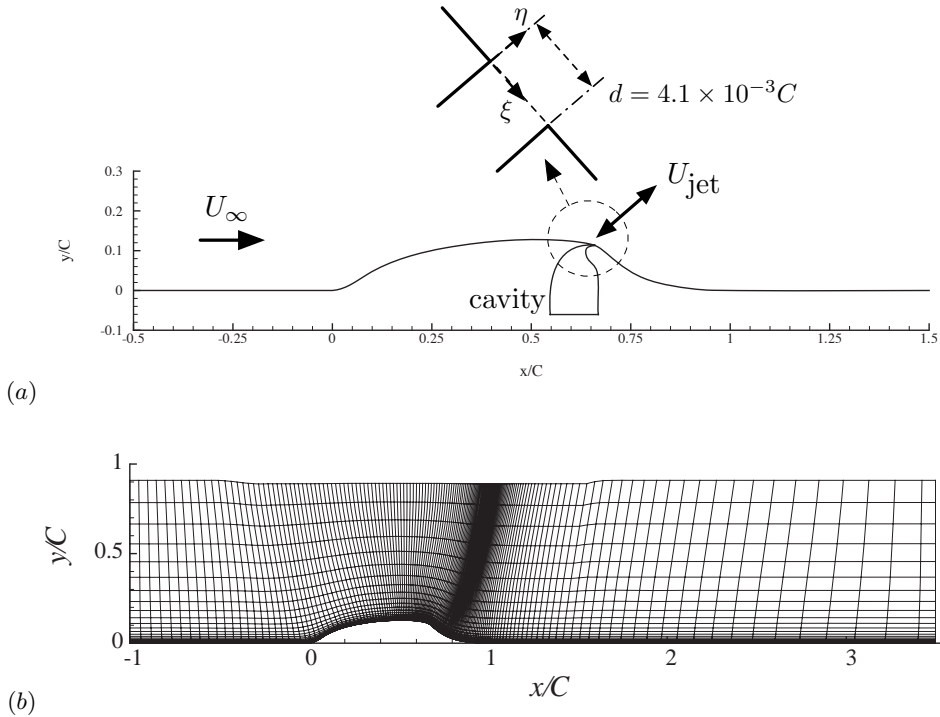


FIGURE 1. (a) Flow configuration for experimental study of flow over a wall-mounted hump and (b) computational domain and mesh in the $x - y$ plane (1/5 mesh lines plotted).

The Smagorinsky coefficient c is dynamically computed employing the procedure proposed by Germano *et al.* (1991)

The temporal integration method used to solve the transformed governing equations is based on a fully-implicit fractional step method which avoids the severe time-step restriction that would occur in the synthetic jet orifice region with an explicit scheme. All terms including cross-derivative diffusion terms are advanced using the Crank-Nicolson method in time and are discretized by the second-order central-difference in space. A Newton iterative method is used to solve the discretized nonlinear equations. The Poisson equation is solved by a hybrid procedure which applies a multigrid method to the curvilinear $x - y$ planes and a Fourier spectral method to the remaining Cartesian direction (see Fig. 1 for coordinate definitions).

The entire code has been parallelized using message passing directives (OpenMP) for shared memory platforms like SGI Origin 2000/3800 and Compaq GS320. Significant effort has been put into optimizing the parallel performance by utilizing cache-management strategies and minimizing data dependency (You *et al.* 2004b).

2.2. Flow configuration

The flow configuration is shown in Fig. 1 along with the computational grid plotted only one in every five grid lines for clarity. This configuration is the third test case considered in the NASA Langley Workshop on CFD Validation of Synthetic Jets and Turbulent Separation Control (Rumsey *et al.* 2004; Seifert & Pack 2002; Greenblatt *et al.* 2004, 2005). The original experiment of Seifert & Pack (2002) has been repeated by Greenblatt *et al.* (2004, 2005) to provide a complete data set that can be readily used for CFD

validations. In this study, the experimental data provided by Greenblatt *et al.* (2004, 2005) is used for validating the present LES results. The hump is the upper surface of a Glauert-Goldschmied type airfoil and has a chord length of $C = 0.42m$, a maximum height of $0.0537m$, and a span of $0.5842m$. A cavity slot is located at approximately 65% chord and is used for producing a steady suction and a zero-efflux oscillatory jet. The boundary layer first experiences an adverse pressure gradient as it approaches the hump. It then accelerates over the front convex portion of the hump where the pressure gradient turns favorable and separates over a relatively short concave section in the aft region due to the strong adverse pressure gradient.

The computational domain is of size $L_x \times L_y \times L_z = 4.5C \times 0.9C \times 0.2C$, where C is the hump chord length. In the present LES, smaller domain sizes than those in the experiment are employed in the streamwise and spanwise directions to reduce the computational cost. The top-wall boundary is located at $y/C = 0.9$ with a slight variation to account for the side-wall blockage effect in the experiment, as recommended by the Workshop (<http://cfdval2004.larc.nasa.gov/case3.html>). The Reynolds number of this flow is 9.36×10^5 based on the hump chord and inflow freestream velocity.

A small slot of width $d = 4.1 \times 10^{-3}C$ across the entire length of the span and located at approximately 65% of the hump chord is used to introduce flow control, using either steady suction with bulk suction velocity of $U_0 = 0.37U_\infty$ or sinusoidal suction/blowing at non-dimensional frequency of $f = 1.6812U_\infty/C$ with peak bulk jet velocity of $U_0 = 0.77U_\infty$, respectively. An important aspect of the present study is that velocity boundary conditions are utilized to realize the control jets instead of simulating the flow inside cavity. This approach significantly reduces the computational cost by avoiding a complicated and time-consuming moving mesh computation. Parabolic velocity profiles of

$$U_{\text{jet}} = 6U_0 \left(\frac{\xi}{d} - \left(\frac{\xi}{d} \right)^2 \right) \quad (2.4)$$

and

$$U_{\text{jet}} = 6U_0 \left(\frac{\xi}{d} - \left(\frac{\xi}{d} \right)^2 \right) \sin(2\pi ft), \quad (2.5)$$

where $0 \leq \xi \leq d$, are used in the normal direction, η , to the slot, for steady suction and sinusoidal oscillatory jet, respectively (see Fig. 1 for definitions of ξ and η coordinates). There is a consensus among the researchers that control effects on the hump flow are mostly unaffected by the alternative choice of velocity boundary conditions for modeling steady suction and synthetic jets (Rumsey *et al.* 2004; Šarić *et al.* 2005; Capizzano *et al.* 2005). The mass flux coefficient of 0.15% and the momentum coefficient based on the peak jet velocity of 0.11%, which are also used in the experiments, are used for steady suction and oscillatory jet cases, respectively.

No-stress and no-slip boundary conditions are applied along the top and bottom walls, respectively. Periodic boundary conditions are used along the spanwise (z) direction. The inflow turbulent boundary layer data are provided from a separate simulation of flat-plate boundary layer using the method of Lund *et al.* (1998) with the boundary layer thickness of $\delta = 0.073C$ at $x/C = -2.14$ as in the experiment. At the exit boundary, the convective boundary condition is applied, with the convection speed determined by the streamwise velocity averaged across the exit plane.

The mesh size used for the present simulation is $721 \times 161 \times 65$ ($x \times y \times z$). 24 mesh points are allocated along the cavity slot. The grid spacings on the wall in the streamwise,

transverse, and spanwise directions are $\Delta x/C \leq 4.1 \times 10^{-2}$, $\Delta y/C \leq 1.74 \times 10^{-5}$, and $\Delta z/C \leq 3.1 \times 10^{-3}$, respectively. The wall resolution is within the range $\Delta x^+ \leq 50$, $\Delta y^+ \leq 0.8$, and $\Delta z^+ \leq 25$. The present resolution is similar to or better than that found in a number of successful LES of separated flows using the present code (You *et al.* 2004a; Wang & Moin 2000; Kaltenbach *et al.* 1999; Mittal & Moin 1997). Prior to this simulation, coarser grid simulations were carried out to determine the resolution requirements, and the final mesh was subsequently constructed using this information.

The simulation is advanced in time with maximum Courant-Friedrichs-Lewy (CFL) number equal to 3 which corresponds to $\Delta t U_\infty / C \approx 0.4 \times 10^{-3}$, and each time step requires a wallclock time of about 20 seconds when 8 CPUs of IBM Power4+ are used. The present results are obtained by integrating the governing equations over an interval of about $10C/U_\infty$.

3. Results and discussion

LES results for the baseline (no control), suction, and oscillatory jet cases are compared to those provided by the experiment (Greenblatt *et al.* 2004, 2005), LES with a constant Smagorinsky model (hereafter denoted by LESC) (Šarić *et al.* 2005), DES (Krishnan *et al.* 2004), URANS (Capizzano *et al.* 2005), and ILES (Morgan *et al.* 2005). Except for the ILES, the previous numerical studies (Šarić *et al.* 2005; Krishnan *et al.* 2004; Capizzano *et al.* 2005) provide only a subset of data with which the present LES results are compared. For instance, only the pressure coefficient is available for the oscillatory case in the URANS. A number of (U)RANS calculations have been made by different researchers (e.g. Refs. Capizzano *et al.* (2005); Morgan *et al.* (2004); Krishnan *et al.* (2004) and see also Ref. Rumsey *et al.* (2004) for the summary of the (U)RANS studies), and their results are qualitatively similar. Here, we use those in Ref. Capizzano *et al.* (2005) as representative solutions for comparison.

Figure 2 shows comparisons of the mean surface pressure coefficients, $-C_p$, which reflect overall features of the flow-field. The flow is accelerated up to around the mid-chord of the hump, where a peak magnitude of $-C_p$ is observed. A sudden drop of $-C_p$ afterwards leads to separation at around $x/C = 0.65$, which corresponds to the location of the cavity slot. All the numerical simulations, including the present LES, LESC, DES, URANS, and ILES, predict reasonably well the hump surface pressure distribution up to the separation point for uncontrolled and controlled cases. Continuous suction and oscillatory jets shorten the recirculation bubble size relative to the uncontrolled case. The superior predictive capability of the present LES is noticeable after the flow separation, where URANS (Capizzano *et al.* 2005) was clearly unable to predict the pressure recovery and the correct separation bubble size. The ILES (Morgan *et al.* 2005) show much better results than does URANS but still deviates from the experimental measurement in the oscillatory case. Morgan *et al.* (2005) suggested that the lower Reynolds number in the ILES reduces the effectiveness of flow control.

Gross features of the flow separation in the uncontrolled and controlled cases are visualized using the streamwise vorticity contours and are shown in Fig. 3. Incoming turbulent boundary layer separates due to the strong adverse pressure gradient near the cavity slot and produces abundant small scale vortices between the separated shear layer and bottom wall (Fig. 3(a)). In Fig. 3(b), it is clear that steady suction weakens the shear layer and reduces the separation bubble size by removing mass flux through the cavity slot. In the oscillatory jet case as shown in Fig. 3(c), a periodic production and

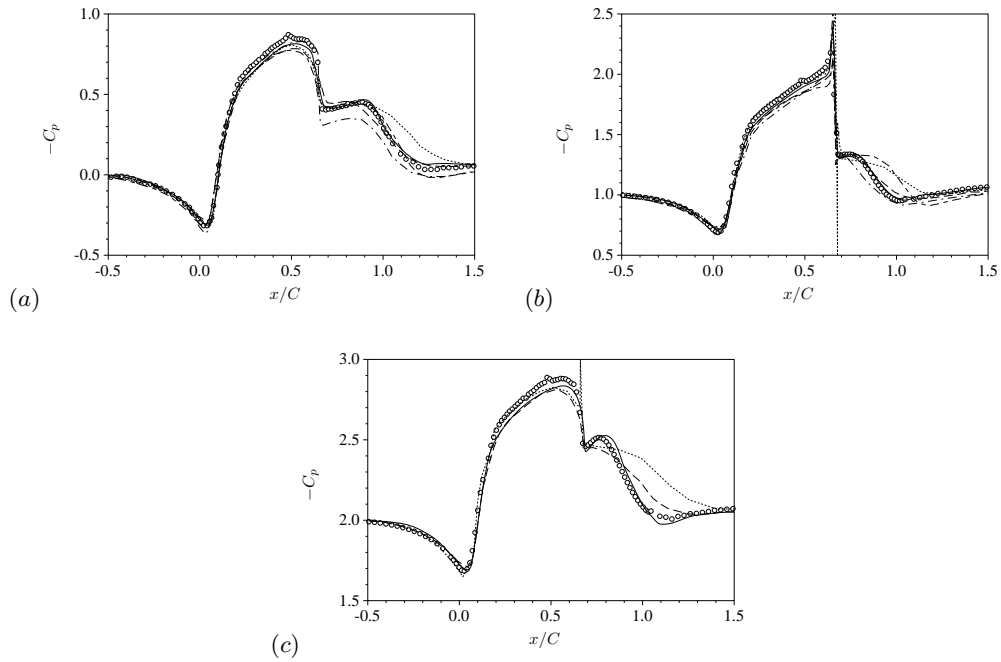


FIGURE 2. Surface pressure coefficient. —, present LES; —·—, LESC (Šarić *et al.* 2005); — — —, DES (Krishnan *et al.* 2004); ·····, URANS (Capizzano *et al.* 2005); - - - - , ILES† (Morgan *et al.* 2005); ○, experiment (Greenblatt *et al.* 2004, 2005). (a) Baseline; (b) steady suction; (c) oscillatory jet.

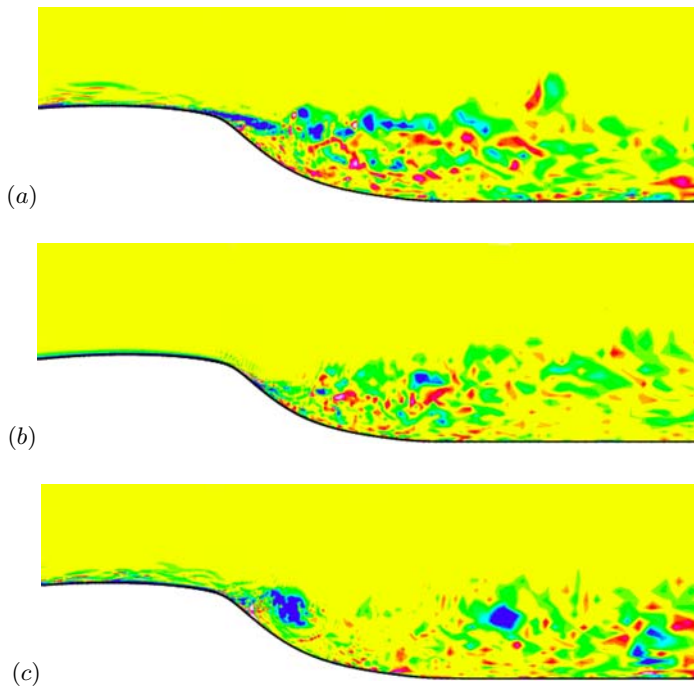


FIGURE 3. Instantaneous streamwise vorticity contours. (a) Baseline; (b) steady suction; (c) oscillatory jet. 20 contour levels in the range of ± 35 are plotted.

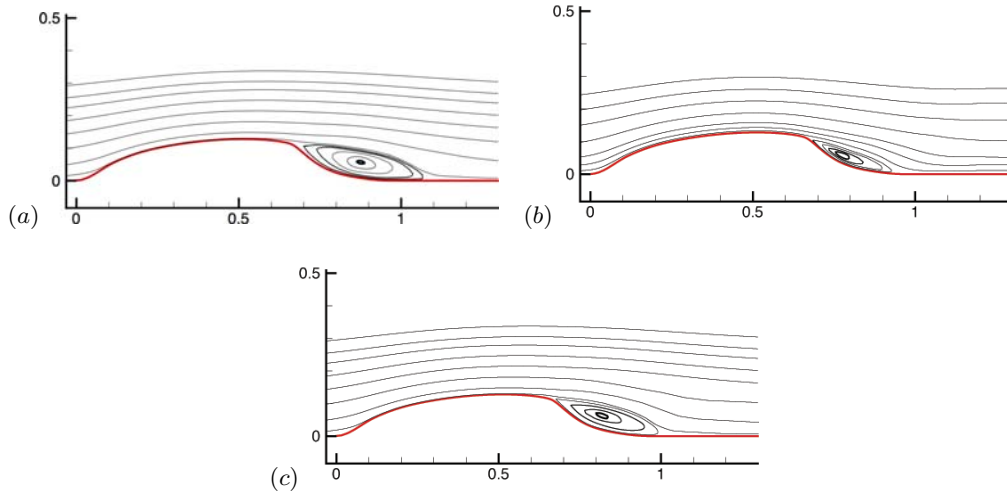


FIGURE 4. Mean streamlines. (a) Baseline; (b) steady suction; (c) oscillatory jet.

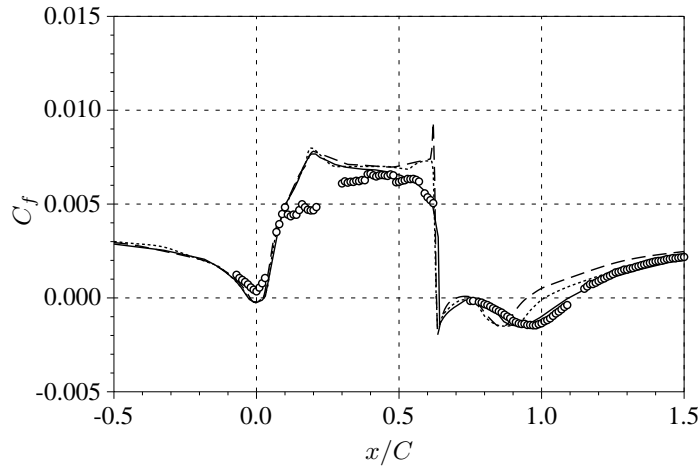


FIGURE 5. Skin friction coefficient predicted by the present LES. — , baseline; ---- , steady suction; ····· , oscillatory jet.

convection of large-scale vortices is observed. The repeated process of vortex roll-up and shedding is also found to reduce effectively the separation bubble size. A comparison of the time-averaged separation bubble sizes predicted by the present LES for the three cases is made in Fig. 4, which also shows qualitatively the effectiveness of control jets in terms of the flow separation and reattachment locations and bubble size. Both the steady suction and oscillatory jets reduce the size of separation bubble as well as the location of the core of flow recirculation.

The effectiveness of steady suction and oscillatory jet on the separation control is more clearly identified in Fig. 5, which shows a comparison of the skin-friction coefficient C_f predicted by the present LES for the uncontrolled and controlled cases. The line $C_f = 0$ delineates the border between separated and reattached flow. In the baseline case, the LES shows favorable agreement with experimental data except for the front convex region of the hump, where the LES over-predicts the skin-friction coefficient. The reattachment

Case	Baseline	Suction	Oscillation
present LES	1.09	0.95	1.01
LESC (Šarić <i>et al.</i> 2005)	1.114	0.947	1.020
DES (Krishnan <i>et al.</i> 2004)	1.13		
URANS (Capizzano <i>et al.</i> 2005)	1.25	1.08	1.15
ILES [†] (Morgan <i>et al.</i> 2005)	1.127	0.984	1.097
Experiment (Greenblatt <i>et al.</i> 2004, 2005)	1.110 ± 0.003	0.94 ± 0.05	0.98

TABLE 1. Locations of flow reattachment behind the hump. [†]A lower Reynolds number of $Re = 2 \times 10^5$ is used.

locations obtained from the present LES are quantitatively compared in Table 3 to other experimental and numerical results for the three cases. The present LES and LES (Šarić *et al.* 2005) clearly yield more accurate predictions of the separation bubble sizes than do any other previous numerical studies. Although the ILES (Morgan *et al.* 2005) showed favorable agreements with experiments for the baseline and steady suction cases, the reattachment length is approximately 10% longer in the oscillatory case. As already observed in the surface pressure distributions, the URANS calculations gave significantly longer reattachment lengths for all three cases. The deficiency of URANS is more clear in the case of oscillatory jet control. In general, RANS models are known to have difficulty in predicting flow separation and unsteady mixing (Rumsey *et al.* 2004).

In Fig. 6, the uncontrolled and controlled mean streamwise velocity profiles are compared to experimental and other numerical data at two streamwise locations, $x/C = 0.8$ and 1.2. Note that not all the mean velocity and turbulence statistics at those two locations are available from other numerical solutions with which the present LES results are compared. Inside the separation bubble at $x/C = 0.8$, the LES profiles show best match with the experimental data, although other numerical simulations also show favorable agreements. The velocity profiles indicate that the separation bubble is decreased by both the steady suction and oscillation. In relative terms, the suction is more effective than the oscillatory jet in reducing the separation bubble size, as also shown in Figs. 4 and 5 and Table 3. At a location slightly downstream of flow reattachment ($x/C = 1.2$), the agreement between the present LES and experimental data is quite good, while the LES and DES could not correctly predict the velocity profiles in the oscillatory jet and suction cases, respectively. The LES shows favorable predictions that are comparable to the present LES results in the baseline and steady suction cases. The DES produces a marginal result in the baseline case, although it clearly fails in predicting the mean velocity profile in the suction case. The URANS and ILES show profiles which are not

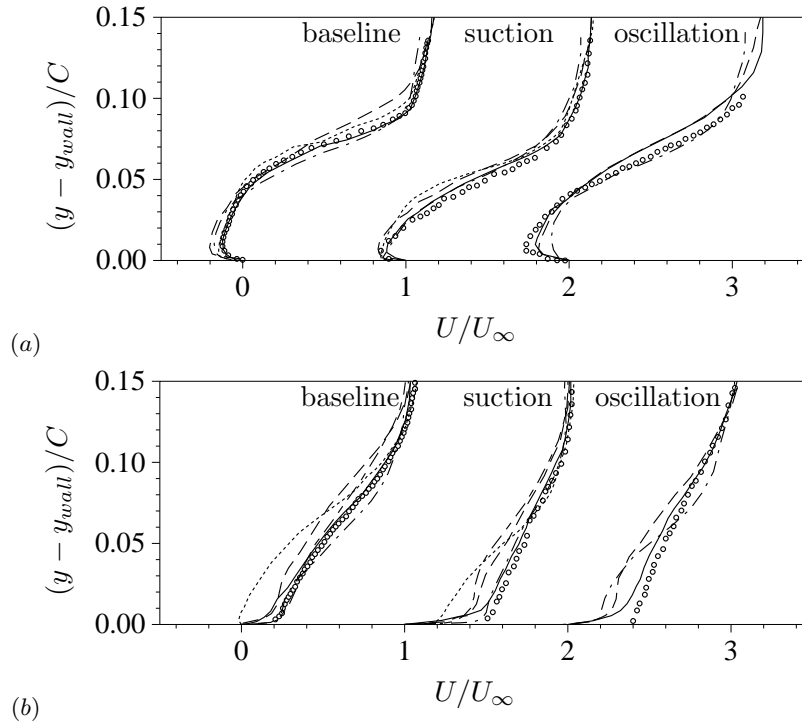


FIGURE 6. Mean streamwise velocity profile. (a) $x/C = 0.8$; (b) $x/C = 1.2$. —, present LES; —·—, LESC (Šarić *et al.* 2005); ----, DES (Krishnan *et al.* 2004); ·····, URANS (Capizzano *et al.* 2005); - - - - , ILES[†] (Morgan *et al.* 2005); ○, experiment (Greenblatt *et al.* 2004, 2005). The profiles for the suction and oscillation cases are shifted by 1 and 2, respectively.

as fully recovered as in the experiment due to delayed reattachment. Overall, there is a consistent trend in that the streamwise velocity profiles are fuller in the cases with flow control. The mean velocity profile in the suction case is the fullest due to the earliest flow reattachment.

Comparisons of turbulent kinetic energy (TKE) obtained from the present LES and other numerical and experimental studies are shown in Fig. 7 at the same two streamwise locations, $x/C = 0.8$ and 1.2 , where the mean streamwise velocity profiles are compared. The superior predictive capability of the present LES is again evident. For uncontrolled and controlled cases, the LES results agree reasonably well with the experimental data and are better than those from URANS and ILES. The ILES shows a reasonable agreement with the experimental data in the controlled cases, but worse results than URANS in the baseline case. Inside the separation bubble, the peak TKE is found closer to the wall in the suction and oscillatory cases compared to the baseline case. This is an indication of the control effect on the turbulent mixing. Larger TKE is observed inside the bubble than in the reattached region downstream. At $x/C = 1.2$, larger TKE magnitudes are found in the baseline and oscillatory cases than in the suction case, which is related to the larger sizes of the separation bubbles in the former cases.

The Reynolds stress profiles from numerical simulations and experiments are compared in Fig. 8. In general, the present LES is consistently better in predicting the Reynolds shear stress in the uncontrolled and controlled cases. The LESC results deviate from the experimental data in the baseline case, while the results are in good agreement

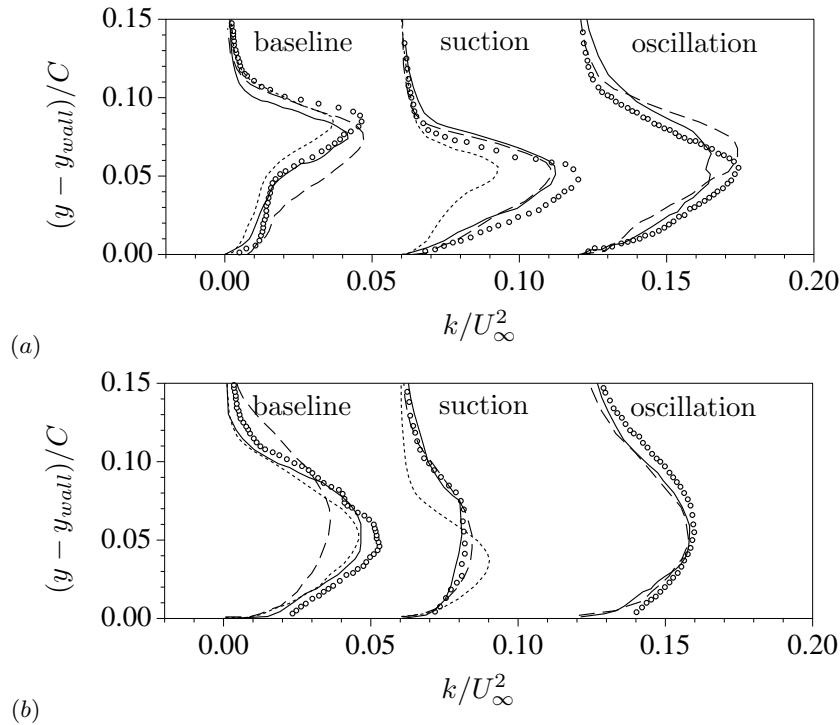


FIGURE 7. Turbulent kinetic energy profile. (a) $x/C = 0.8$; (b) $x/C = 1.2$. —, present LES; ·····, URANS (Capizzano *et al.* 2005); ----, ILES (Morgan *et al.* 2005); \circ , experiment (Greenblatt *et al.* 2004, 2005). The profiles for the suction and oscillation cases are shifted by 0.06 and 0.12, respectively.

with experimental data in the suction case. It is well known that LES with a single constant model coefficient such as the one employed in the study of Šarić *et al.* (2005) is generally unable to represent consistently the correct subgrid-scale stress in various flow situations (Germano *et al.* 1991). The URANS results significantly under-predict the peak magnitude of the Reynolds shear stress, particularly inside the separation bubble. This under-prediction is consistent with the delayed reattachment, since it indicates reduced turbulent mixing inside the separated region. The results from ILES are consistent with its turbulent kinetic energy predictions, showing better agreements with experimental data in the controlled cases and poor agreement in the baseline case.

4. Conclusions

Large-eddy simulation with a dynamic subgrid-scale model and non-dissipative numerics has been employed to predict the turbulent flow separation and its control by synthetic jets over a wall-mounted hump. Results from the present LES for the uncontrolled and controlled cases are compared to experimental data and previous computational predictions using LES with a constant coefficient Smagorinsky model, DES, URANS and ILES. The present LES is shown to be consistently more accurate than the previous numerical approaches. It predicts well the experimentally measured flow quantities such as the pressure coefficient, reattachment length, mean velocity, and turbulence statistics. The reattachment points downstream of the hump are predicted accurately for all three cases.

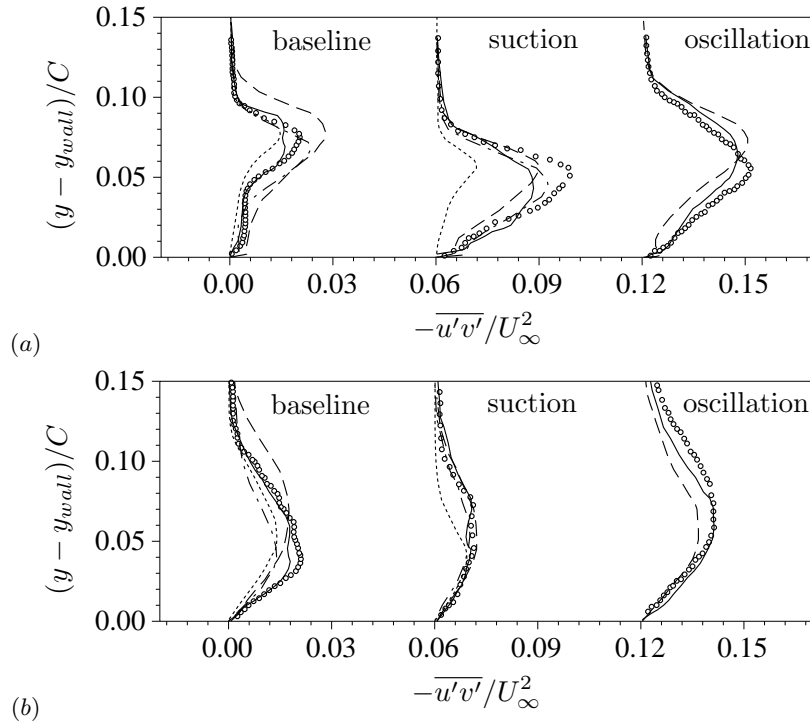


FIGURE 8. Reynolds shear stress profile. (a) $x/C = 0.8$; (b) $x/C = 1.2$. —, present LES; — · —, LES_C (Šarić *et al.* 2005); ·····, URANS (Capizzano *et al.* 2005); ----, ILES[†] (Morgan *et al.* 2005); o, experiment (Greenblatt *et al.* 2004, 2005). The profiles for the suction and oscillation cases are shifted by 0.06 and 0.12, respectively.

It is also shown that steady suction and synthetic jet oscillations cause a reduction of the reattachment length by 7 ~ 13%, compared to the uncontrolled case.

Acknowledgments

The authors acknowledge support from Boeing company and the valuable discussions with Dr. Arvin Shmilovich.

REFERENCES

- BEAUDAN, P. & MOIN, P. 1994 Numerical experiments on the flow past a circular cylinder at sub-critical Reynolds number. *Report TF-62*. Department of Mechanical Engineering, Stanford University, Stanford, California.
- CAPIZZANO, F., CATALANO, P., MARONGIU, C. & VITAGLIANO, P. L. 2005 U-RANS modelling of turbulent flows controlled by synthetic jets. *AIAA-2005-5015*.
- CHOI, H., MOIN, P. & KIM, J. 1992 Turbulent drag reduction: studies of feedback control and flow over riblets. *Report TF-55*. Department of Mechanical Engineering, Stanford University, Stanford, California.
- GERMANO, M., PIOMELLI, U., MOIN, P. & CABOT, W. H. 1991 A dynamic subgrid-scale eddy-viscosity model. *Phys. Fluids*. **3**, 1760–1765.
- GLEZER, A. & AMITAY, M. 2002 Synthetic jets. *Ann. Rev. Fluid Mech.* **34**, 503–529.

- GREENBLATT, D., PASCHAL, K. B., YAO, C.-S. & HARRIS, J. 2005 A separation control CFD validation test case part 2. zero efflux oscillatory blowing. *AIAA-2005-0485*.
- GREENBLATT, D., PASCHAL, K. B., YAO, C.-S., HARRIS, J., SCHAEFFLER, N. W. & WASHBURN, A. E. 2004 A separation control CFD validation test case part 1. baseline & steady suction. *AIAA-2004-2220*.
- KALTENBACH, H.-J., FATICA, M., MITTAL, R., LUND, T. S. & MOIN, P. 1999 Study of flow in a planar asymmetric diffuser using large-eddy simulation. *J. Fluid Mech.* **390**, 151–185.
- KRISHNAN, V., SQUIRES, K. D. & FORSYTHE, J. R. 2004 Prediction of separated flow characteristics over a hump using RANS and DES. *AIAA-2004-2224*.
- LUND, T. S., WU, X. & SQUIRES, K. D. 1998 Generation of turbulent inflow data for spatially-developing boundary layer simulations. *J. Comp. Phys.* **140**, 233–258.
- MITTAL, R. & MOIN, P. 1997 Suitability of upwind-biased schemes for large-eddy simulation of turbulent flows. *AIAA J.* **36**, 1415–1417.
- MORGAN, P. E., RIZZETTA, D. P. & VISBAL, M. R. 2004 Numerical investigation of separation control for flow over a wall-mounted hump. *AIAA-2004-2510*.
- MORGAN, P. E., RIZZETTA, D. P. & VISBAL, M. R. 2005 Large-eddy simulation of separation control for flow over a wall-mounted hump. *AIAA-2005-5017*.
- POSTL, D., WERNZ, S. & FASEL, H. 2004 Case 3: direct numerical simulation on the Cray X1. In *NASA Langley Workshop on CFD Validation of Synthetic Jets and Turbulent Separation Control*.
- RUMSEY, C. L., GATSKI, T. B., SELLERS III, W. L., VATSA, V. N. & VIKEN, S. A. 2004 Summary of the 2004 CFD validation workshop on synthetic jets and turbulent separation control. *AIAA-2004-2217*.
- ŠARIĆ, S., JAKIRLIĆ, S. & TROPEA, C. 2005 Computational analysis of locally forced flow over a wall-mounted hump at high-Re number. In *Fourth Int'l Symp. Turbulence Shear Flow Phenomena* (ed. J. A. C. Humphrey, J. K. Eaton, R. Friedrich, N. Kasagi, M. A. Leschziner & T. B. Gatski), 1189–1194.
- SEIFERT, A. & PACK, L. G. 2002 Active flow separation control on wall-mounted hump at high Reynolds numbers. *AIAA J.* **40**, 1363–1372.
- WANG, M. & MOIN, P. 2000 Computation of trailing-edge flow and noise using large-eddy simulation. *AIAA J.* **38**, 2201–2209.
- WU, X. & SQUIRES, K. D. 1998 Numerical investigation of the turbulent boundary layer over a hump. *J. Fluid Mech.* **362**, 229–271.
- YOU, D., MITTAL, R., WANG, M. & MOIN, P. 2004a Computational methodology for large-eddy simulation of tip-clearance flows. *AIAA J.* **42**, 271–279.
- YOU, D., MOIN, P., WANG, M. & MITTAL, R. 2004b Study of tip clearance flow in a turbomachinery cascade using large eddy simulation. *Report TF-86*. Department of Mechanical Engineering, Stanford University, Stanford, California.